Piezoelectricity of Functionalized Graphene: A Quantum-Mechanical Rationalization

Piezoelectricity of Functionalized Graphene: A Quantum-mechanical Rationalization

Khaled E. El-Kelany,[*,†] Philippe Carbonnière,[*,†] Alessandro Erba,[¶] Jean-Marc Sotiropoulos,[†] and Michel Rérat[†]

Equipe de Chimie Physique, IPREM UMR5254, Université de Pau et des Pays de l'Adour, 64000 Pau, France, Chemistry Department, Faculty of Science, Minia University, Minia 61519, Egypt, and Dipartimento di Chimica and Centre of Excellence NIS (Nanostructured Interfaces and Surfaces), Università di Torino, via Giuria 5, IT-10125 Torino, Italy

E-mail: khaled.el-kelany@univ-pau.fr; philippe.carbonniere@univ-pau.fr

[*]To whom correspondence should be addressed

[†]Equipe de Chimie Physique, IPREM UMR5254, Université de Pau et des Pays de l'Adour, 64000 Pau, France

[‡]Chemistry Department, Faculty of Science, Minia University, Minia 61519, Egypt

[¶]Dipartimento di Chimica and Centre of Excellence NIS (Nanostructured Interfaces and Surfaces), Università di Torino, via Giuria 5, IT-10125 Torino, Italy

Abstract

A large out-of-plane piezoelectricity can be induced in graphene by carbon substitution. Several simple substitutions are considered where C atoms are replaced by heavier group-IV elements (Si, Ge and Sn). A more complex functionalization (namely, pyrrolic N-doped graphene) is also investigated where different functional groups, such as F, Cl, H_3C and H_2N, are studied. Piezoelectric and elastic response properties of all systems are determined quantum-mechanically at the *ab initio* level of theory. A rationalization of the physical and chemical parameters which most affect the out-of-plane piezoelectricity of functionalized graphene is reported, which reveals the dominant character of the nuclear over electronic contribution. The combination of an out-of-plane symmetry-breaking defect and a soft infrared-active phonon mode, with a large cell-deformation coupling, is shown to constitute the necessary prerequisite to induce a large out-of-plane piezoelectric response into functionalized graphene.

Introduction

Piezoelectricity consists in the mutual conversion of mechanical and electrical forces in the material and, since its discovery in 1880, it is central to a wide variety of technological applications: next-generation energy harvesters,[1,2] artificial muscles,[3] sensors and actuators, etc.[4] One obvious limitation of such an important property is that of being restricted to non-centrosymmetric crystals. In this respect, it has recently been shown that a reduction of the dimensionality of bulk materials represents an effective way of enhancing (or even creating) a piezoelectric response:[5] for instance, single-layered 2D materials such as *h*-BN, *h*-MoS_2 and *h*-WS_2 do show a piezoelectric effect while their 3D bulk analogs do not.[6–8]

When it comes to low-dimensional systems, graphene would clearly be the most promising material to work with in the fabrication of electronic, optoelectronic and spintronic nano-devices due to all of its well-known remarkable properties, including extraordinarily high electron mobility, mechanical stiffness and flexibility.[9–15] The exploitation of piezoelectricity of graphene would indeed lead to a new branch of possible applications in nano-electro-mechanical systems (NEMS)

devices requiring high electromechanical coupling. Unfortunately, graphene possesses an inversion symmetry center in its undistorted D_{6h} equilibrium configuration, which prevents a piezoelectric response to take place in its pristine form. However, its inversion center can be broken and piezoelectricity engineered by several means including adsorption, hole creation, application of biaxial strain, chemical doping, etc.[16–21] A large out-of-plane piezoelectric response has recently been measured for a graphene single layer as deposited on a SiO_2 substrate.[20]

Among other strategies to induce a piezoelectric response in graphene, chemical doping seems the most promising as it already represents an effective experimental mean for tuning its structural and electronic properties.[22,23] Free-standing BN-, N-, B-, and Si-doped graphene monolayers have recently been synthesized and found to be chemically stable at ambient conditions.[24–27] Furthermore, both dopant concentration and spatial configuration have recently been shown to be tunable, to some extent.[28,29] For instance, N-doped graphene exhibits three common bonding configurations: pyridinic, pyrrolic and graphitic, whose relative occurrence is systematically affected by several factors of the chemical-vapor-deposition process: precursor, catalyst, flow rate, and growth temperature.[29] Hydrothermal reduction of colloidal dispersions of graphite oxide in the presence of hydrazine is an alternative approach to selectively obtain pyrrolic N-doped graphene,[30] while a solvo-thermal synthesis via the reaction of tetrachloromethane with lithium nitride under mild conditions leads to production in gram scale.[31]

In a recent study, we have systematically investigated the in-plane piezoelectric response of graphene as induced by several inversion symmetry-breaking defects and found a peculiar "universal" behavior: a common finite in-plane piezoelectric response (characterized by a direct piezoelectric coefficient e_{11} of about 5×10^{-10} C/m) in the limit of vanishing defect concentration, thus highlighting an intrinsic nature of the piezoelectric activity of graphene.[21]

The present investigation aims at providing a complete quantum-mechanical rationalization of the overall (in-plane and out-of-plane) piezoelectric effect as induced in graphene by any inversion symmetry-breaking defect. While confirming the "universal" in-plane behavior, the atomistic mechanisms behind a possible giant out-of-plane piezoelectricity are here addressed and under-

stood. Different kinds of chemical doping are considered (Si, Ge, Sn, pyrrolic N), which can lead to an out-of-plane piezoelectric response up to 300 times larger than the largest one reported so far in the literature for free-standing graphene (which was obtained by adsorption of Li atoms on the graphene surface).[16]

In an ideally planar structure, out-of-plane response properties would clearly be ill-defined. However, when carbon atoms are chemically substituted with Si, Ge or Sn ones, local protrusions are formed due to their different size, which reduce the symmetry of the resulting system to non-centrosymmetric, non-planar C_s. Also pyrrolic N-doped graphene (H-NG in the following) exhibits an out-of-plane response given that the NH functional group points out of graphene plane. Substitution of H with different functional groups, such as halogen (F, Cl), methyl (H_3C) and amino (H_2N) ones, is additionally investigated, which results in the softening of phonon modes and enhancing of the piezoelectric response. The effect of defect concentration is investigated in at least one case while the separate electronic and nuclear contributions to the total piezoelectric response are discussed for all defects. Elastic features of most structures are also investigated.

Theoretical and Computational Aspects

The elements e_{iv} of the third-rank direct piezoelectric tensor can be defined as second energy H derivatives with respect to Cartesian components E_i of an applied electric field and components η_v of the strain tensor. According to quantum-mechanical perturbation theory, piezoelectricity can then be represented as a sum of fractional terms that have slightly different forms for the electronic and vibrational contributions. The electronic contribution can be written as:

$$e_{iv}^{\mathrm{ele}} \propto 2 \sum_{n \neq 0} \frac{(\mu_i)_{0\to n}(-\frac{\partial H}{\partial \eta_v})_{0\to n}}{(\Delta\varepsilon)_{0\to n}} \,, \tag{1}$$

where the numerator is the product of allowed transition moments $(\mu)_{0\to n}$ and $(-\frac{\partial H}{\partial \eta})_{0\to n}$ due to the electric and mechanical fields, respectively, and where $\mu = -\partial H/\partial E$ is the dipole moment. The denominator $(\Delta\varepsilon)_{0\to n}$ is an energy difference between the ground Ψ_0 and excited Ψ_n

spectroscopic state (eigenvector of the unperturbed Schrödinger equation). Thus, the electronic contribution to piezoelectricity is dominated by the denominator of the above expression, and so by the electronic band gap, if the corresponding transition is symmetry-allowed. The vibrational contribution can be expressed as:

$$e_{iv}^{\text{vib}} \propto \sum_{p} \frac{\frac{\partial \mu_i}{\partial Q_p}\left(-\frac{\partial^2 H}{\partial \eta_v \partial Q_p}\right)}{\omega_p^2} , \tag{2}$$

where the sum runs over phonon modes, Q_p is the harmonic normal mode coordinate and ω_p the corresponding phonon frequency. The numerator of the above equation essentially contains the allowed transition moments induced by a vibrational motion, with respect to the electric and mechanical fields as for the electronic contribution. From the sole formal analysis of equation (2), the large contribution of a soft (i.e. with small ω_p) infrared-active (i.e. with $\frac{\partial \mu_i}{\partial Q_p} \neq 0$) phonon mode to piezoelectricity is clear.

The adopted computational strategy consists in computing the intensity of polarization induced by an applied strain, according to the Berry phase approach,[32–34] as implemented[35,36] in the CRYSTAL14 program[37,38] that is here used for all calculations. The global hybrid B3LYP functional[39] of the density-functional-theory (DFT) is chosen in combination with an atom-centered all-electron basis set of triple-ξ quality, augmented with polarization functions for all atoms,[40] apart from Sn for which a Durand effective pseudo-potential is used.[41] Our previous investigation of in-plane piezoelectricity of graphene documented the little dependence of the computed response on the particular adopted functional.[21]

In the linear regime, direct **e** and converse **d** piezoelectric tensors describe the polarization induced by strain and the strain induced by an external electric field, respectively; a simple connection exists between the two (**e** = **d** $\mathbb{C}$ or **d** = **e** $\mathbb{S}$) via the elastic tensor $\mathbb{C}$ and its inverse $\mathbb{S} = \mathbb{C}^{-1}$. Elastic constants and related properties are computed as strain numerical derivatives of analytical energy gradients with the fully-automated procedure implemented in the CRYSTAL14 program for the evaluation of fourth-rank elastic, photo-elastic and piezo-optic tensors.[42–45]

The level of accuracy in evaluating the Coulomb and exact exchange infinite lattice series is controlled by five thresholds set to T_1=T_2=T_3=T_4=1/2T_5=8.[38] Reciprocal space is sampled according to a regular Pack-Monkhorst sub-lattice with a shrinking factor of 42, corresponding to 463 independent **k**-points in the first irreducible Brillouin zone. We recently utilized the same computational approach for investigating the piezoelectric response of 3D systems such as $SrTiO_3$,[36] $BaTiO_3$,[46] Ge-doped quartz,[47] and low-dimensional systems such as *h*-BN,[48] *h*-ZnO,[49] and BeO nanotubes.[50] An alternative analytical approach, based on the Coupled-Perturbed-Hartree-Fock/Kohn-Sham (CPHF/KS) scheme, has recently been implemented in a development version of the CRYSTAL14 program for the calculation of direct piezoelectricity of 3D crystals.[51]

Results and Discussion

As mentioned in the Introduction, a small out-of-plane piezoelectric response can be induced in graphene by the one-sided adsorption of light atoms on its surface.[16] In this section, we investigate the much larger piezoelectricity obtained by substituting carbon with other group-IV elements (Si, Ge, Sn) or by N-doping in the pyrrolic configuration. A graphical representation of the equilibrium nuclear configurations of such functionalized graphenes is given in Figure 1. Due to their larger size, bond lengths between substituted atoms and their first-neighbors are increased by 18, 23 and 50% with respect to pristine graphene for Si, Ge and Sn, respectively. Furthermore, substituted atoms arrange into an out-of-plane equilibrium configuration, where an angle δ can be defined to describe the amount of their protrusion from the plane ($\delta = 4.5^\circ$, 11.4° and 42.1° along the series). In the case of pyrrolic N-doped graphene, the carbon atoms of highly stressed five-membered rings lie on the plane while nitrogen atoms lie out of the plane by an angle $\delta = 15.3^\circ$. Note that in pyrrolic N-doped graphene, asymmetric holes are formed, which further reduce the symmetry of the system to C_1. In all cases, one-sided configurations only are considered as was done in previous investigations on atom adsorptions, because equally distributed two-sided configurations would obviously imply a null average out-of-plane piezoelectric response.[16] Due to the low C_s or

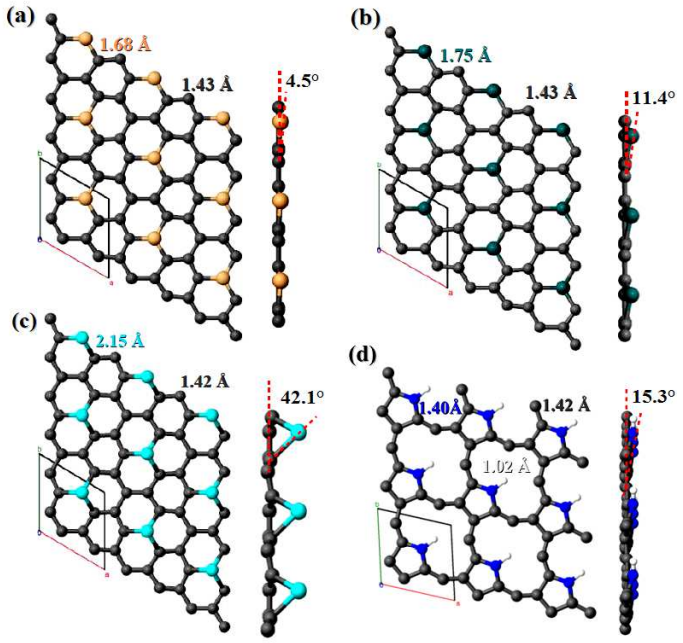

Figure 1: (color online) The equilibrium structure of Si-, Ge-, Sn- and pyrrolic N-doped graphene is shown in panels a, b, c and d, respectively. For each configuration, top and lateral views are reported, where the deformation angle δ (in degrees) and bond lengths (in Å) are also given. The unit cell used in the calculation is displayed for each configuration.

C_1 point-symmetry of these structures, the number of symmetry-independent components of the third-rank direct piezoelectric tensor **e** would be 5 and 9, respectively. However, it turns out that for all structures $e_{11} \simeq -e_{12} \simeq -e_{26}$, $e_{31} \simeq e_{32}$ within approximately 1% and all other constants are almost null. For this reason and for clarity-sake, in what follows we will restrict our discussion to just two piezoelectric coefficients: e_{11} for in-plane and e_{31} for out-of-plane responses.

In-plane Piezoelectricity

We have recently investigated the in-plane piezoelectric response of functionalized-graphene as induced by different patterns of BN domains and by creation of asymmetric holes of different shapes. A "universal" behavior was discovered, characterized by a common direct piezoelectric constant e_{11} of about 5×10^{-10} C/m in the limit of vanishing defect concentration.[21] Before addressing the out-of-plane response of the present functionalized graphenes, let us briefly discuss their in-plane features and prove once more the general validity of the above-mentioned "universal" behavior. To

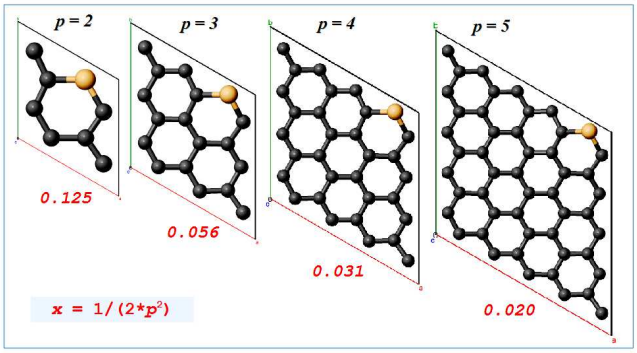

Figure 2: (color online) The four super-cells used to investigate the effect of the substitutional fraction x of carbon with Si, Ge and Sn atoms. The value of p for each model is given.

do so, the piezoelectricity of Si-, Ge- and Sn-doped graphene has been investigated as a function of the substitutional fraction x. Four super-cells have been considered corresponding to four doping concentrations (a graphical representation of the four models is given in Figure 2). From inspection of the figure, x can be expressed as a function of the integer p, which measures the length of the lattice parameters in units of the total number of atomic C-C chains contained in the unit cell ($x = 1/2p^2$).

Table 1 reports the computed values of e_{11} (total and purely vibrational contributions) as a function of defect concentration x for the three different chemical functionalizations. By looking at the total values of the direct piezoelectric constant, it is seen that for small dopant concentrations the common asymptotic value of approximately 5×10^{-10} C/m is reached for all systems,

Table 1: In-plane direct piezoelectric constant e_{11} of Si-, Ge- and Sn-doped graphene as a function of the substitutional fraction x. Total values e_{11}^{tot} and purely vibrational contributions e_{11}^{vib} are reported (in units of 10^{-10}C/m).

	Si		Ge		Sn	
x	e_{11}^{tot}	e_{11}^{vib}	e_{11}^{tot}	e_{11}^{vib}	e_{11}^{tot}	e_{11}^{vib}
0.125	4.01	-1.23	4.22	-0.81	29.15	-8.81
$0.05\overline{6}$	5.45	-1.00	7.63	-0.71	11.78	-0.54
0.031	4.37	-1.90	4.86	-1.35	4.32	-1.36
0.020	4.97	-1.19	4.60	-1.71	4.56	-2.00

despite rather different starting values at high concentrations (particularly so for the Sn doping). It might also be noticed that the computed piezoelectric constant is not monotonously varying as a function of defect concentration. The origin of this behavior is discussed in-depth in our previous investigation about the in-plane response.[21] Let us just briefly recall that this is due to the fact that the band gap of the system varies with defect concentration according to two distinct behaviors depending on whether the considered superlattice is or not a multiple of 3 of the primitive cell of pristine graphene, as predicted by the energy band-folding model.[52–54] As a further consideration, we might notice that the vibrational contribution is always smaller in absolute value than the electronic one, which is found to dominate the in-plane piezoelectric response of functionalized graphene.

Out-of-plane Piezoelectricity

At variance with the in-plane piezoelectric response, we shall here illustrate how the out-of-plane response is entirely dominated by the vibrational contribution, the electronic one being almost null for the following reason: while the transition energy at the denominator of equation (1) is never null, even in the limit of an infinite defect dilution, the vertical transition moments, which constitute the numerator of equation (1), would be null in the ideal planar structure and are always tiny even in the distorted structures. As introduced in Section , the vibrational contribution to the piezoelectricity is dominated by soft IR-active phonon modes. For instance, such a soft vibration mode was shown to entirely account for the giant piezoelectric response of the $SrTiO_3$ perovskite in its ferroelectric phase,[36] which is stable at very low temperatures (below approximately 24 K).[55] In this respect, an obvious advantage of functionalized graphene is that of being stable at ambient conditions.

In Table 2, we report the out-of-plane direct and converse piezoelectric constants of Si-doped graphene as a function of defect concentration x. Total and purely vibrational contributions are given. We observe that: i) the vibrational contribution accounts for 99.98% of the total effect in all cases; ii) out-of-plane piezoelectricity is much larger than the in-plane one (absolute values of the

Table 2: Out-of-plane direct e_{31} and converse d_{31} piezoelectric constants of Si-doped graphene as a function of the substitutional fraction x. Total values and purely vibrational contributions are reported (in units of 10^{-10}C/m and pm/V for direct and converse constants, respectively).

	Direct		Converse	
x	e_{31}^{tot}	e_{31}^{vib}	d_{31}^{tot}	d_{31}^{vib}
0.125	37.50	37.48	12.70	12.68
$0.05\overline{6}$	20.51	20.47	8.16	8.15
0.031	13.92	13.89	4.87	4.86
0.020	11.08	11.06	3.74	3.70

e_{31} versus the e_{11} constant); iii) contrarily to what discussed for the in-plane response, the out-of-plane one systematically decreases as the defect concentration decreases and, eventually, vanishes as far as the limit of infinite defect dilution is reached. We shall now investigate the atomistic origins of such a behavior. To do so, the out-of-plane vibrational motion of substituted atoms has to be characterized: its main features are introduced in the case of Si-doped graphene in Figure 3 as a function of x. Both the vibration mode wavenumber $\bar{\nu}$ and its IR intensity through the z direction $\mathscr{I}_p(z) \propto (\partial\mu_z/\partial Q_p)^2$ are reported, which give an indication about the softness and polarization induced by the mode, respectively. For the largest defect concentration we have considered (x = 0.125), the phonon mode is found to be very soft, with $\bar{\nu}$ = 36 cm^{-1} and to induce a significant polarization, with $\mathscr{I}_p(z)$ = 4 km/mol. As a consequence, it brings a large vibrational contribution to the out-of-plane piezoelectricity, as already documented in Table 2: e_{31} = 37.5 $\times$ 10^{-10} C/m and d_{31} = 12.70 pm/V, values that are 70 times and two orders of magnitude larger than previously reported for Li atoms adsorption on graphene, at the same concentration.[16] As the defect concentration x decreases, the deformation angle δ increases (see panel (b) of Figure 3) and thus the energy required to vertically displace Si atoms increases too (because of the higher penetration barrier it encounters when approaching the graphene plane due to the local rearrangement of the carbon atoms, which "fill" the space left free by the Si atom itself), leading to an increased rigidity of the vibration mode ($\bar{\nu}$ = 36, 207, 271, 257 cm^{-1} along the series). Moreover, the IR intensities per

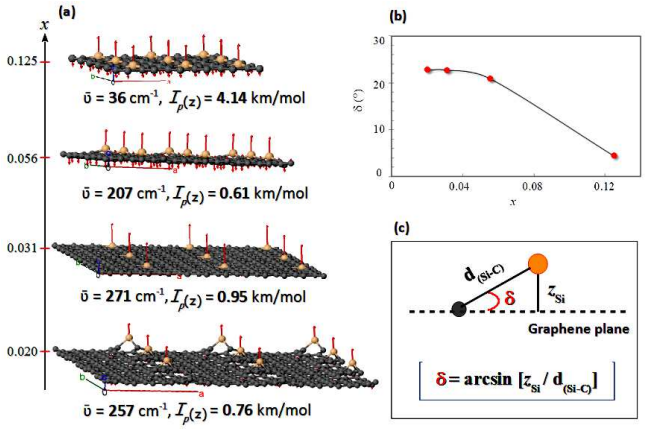

Figure 3: (color online) Graphical representation of the atomic displacements (see red arrows in panel a) involved in the soft phonon mode corresponding to the out-of-plane motion of atoms in Si-doped graphene. Wavenumbers $\bar{\nu}$ and IR intensities $\mathscr{I}_p(z)$ are given for each concentration x. Panel (b) reports the deformation angle δ as a function of x, while panel (c) introduces a graphical definition of δ.

unit cell also decrease with decreasing x, so that eventually the out-of-plane piezoelectric response vanishes for very small x. To summarize, as regards the out-of-plane piezoelectric response, the higher the defect concentration, the more enhanced the piezoelectric activity.

Similar trends are observed also for the other functionalizations: the vibrational contribution dominates the out-of-plane response, which is progressively reduced as x decreases. In Figure 4, we report the values of direct e_{31} and converse d_{31} piezoelectric constants of Si-, Ge-, Sn- and pyrrolic N-doped graphene, at the $x = 0.125$ defect concentration. For each system, values of the deformation angle δ, wavenumber $\bar{\nu}$ and IR intensity $\mathscr{I}_p(z)$ are also given. From inspection of the figure, Ge-doped graphene is seen to exhibit the largest piezoelectric response among the considered systems, with $e_{31} = 157 \times 10^{-10}$ C/m and $d_{31} = 114$ pm/V. The relatively small deformation angle $\delta = 11.4°$ indeed implies a certain softness of the phonon mode ($\bar{\nu} = 115$ cm^{-1}) and allows for Ge atoms to approach the graphene plane so as to induce a significant polarization, reflected in an IR intensity of approximately 2 km/mol.

Based on the analysis we have made so far, it might be striking that Ge-doped graphene exhibits a higher piezoelectricity than Si-doped graphene, being characterized by a less soft phonon mode (i.e. larger $\bar{\nu}$) with a lower induced polarization (i.e. lower $\mathscr{I}_p(z)$). This is due to the fact that

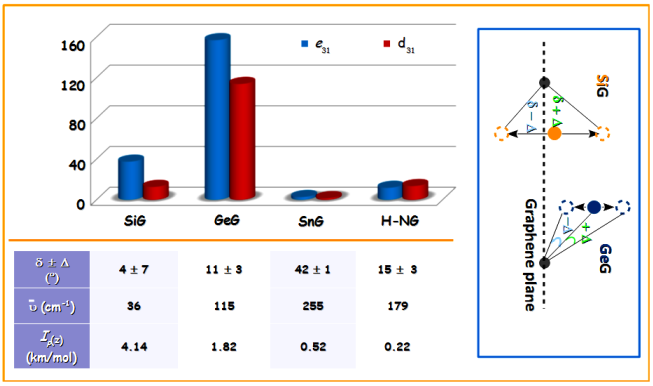

Figure 4: (color online) Direct e_{31} (in units of 10^{-10} C/m) and converse d_{31} (in units of pm/V) piezoelectric constants of functionalized graphenes at the $x = 0.125$ defect concentration. Values of deformation angle δ (as corrected for zero-point motion, $\pm\Delta$), wavenumber $\bar{\nu}$, and IR intensity are given. The vertical inset on the right of the figure gives a graphical representation of how the deformation angle δ is affected by the zero-point motion effect Δ.

the third term of equation (2) has not yet been taken into proper account: $\partial^2 H/(\partial\eta_v \partial Q_p)$, which represents the coupling between the phonon vibration mode and the in-plane deformation. Without this further term, indeed, equation (2) would almost reduce to the expression of the vibrational contribution to the diagonal elements of the polarizability tensor of the system:

$$\alpha_{ii}^{\mathrm{vib}} \propto \sum_p \frac{(\partial\mu_i/\partial Q_p)^2}{\omega_p^2} \,. \tag{3}$$

By restricting the analysis to this quantity, a much larger vibrational contribution to the polarizability of Si- over Ge-doped graphene is observed: $\alpha_{zz}^{\mathrm{vib}}$ = 85.22 and 3.84 a.u., respectively. On the contrary, the above-mentioned coupling is found to be almost null (thus suppressing the out-of-plane piezoelectric response) in Si-doped graphene and much larger in Ge-doped graphene. This coupling between the in-plane lattice deformation and the out-of-plane phonon mode can be interpreted in terms of the atomic displacements involved in the vibration mode (see inset on the right of Figure 4). In the equilibrium configuration of Si-doped graphene, Si atoms are only slightly protruded out of the plane, by a small angle $\delta = 4°$, while the amplitude Δ of their vibrational motion is much larger (7°) even at 0 K (Δ corresponds to the "classical amplitude" of the harmonic oscillator associated with the soft phonon mode). As a result, Si atoms are oscillating across the

graphene plane with a highly symmetric motion, which implies a small coupling with the in-plane deformation (indeed such a coupling would be null by symmetry for an atom lying exactly on the graphene plane). The case of Ge-doped graphene is different as, in its equilibrium configuration, Ge atoms lie well above the graphene plane ($\delta = 11^\circ$) in such a way that, even by accounting for their vibration motion ($\Delta = 3^\circ$), they are likely to remain on just one side of the plane (see again inset of Figure 4), which yields to a large coupling with the in-plane deformation (in other words, the application of an in-plane strain would significantly affect the vertical motion of the Ge atom, which, when approaching the graphene plane, would interact with a rather different local configuration with respect to the unstrained lattice). A further confirmation to this picture (i.e. to the larger value of the coupling between the soft out-of-plane phonon mode and the in-plane deformation in Ge-doped than in Si-doped graphene) comes from the analysis of the vibrational term of the elastic constants of the two systems. Indeed, such a term can be expressed as a sum of phonon mode-specific contributions as (for diagonal C_{vv} constants):[56]

$$C_{vv}^{\text{vib}} \propto \sum_p -\frac{\left(\frac{\partial^2 H}{\partial \eta_v \partial Q_p}\right)^2}{\omega_p^2}\,, \tag{4}$$

where the numerator is precisely the square of the coupling of equation (2). It follows that the analysis of the vibrational contribution of the C_{11} and C_{22} elastic constants could give a clear indication of the relative magnitude of the coupling in the two systems. In Table 3, we report the elastic constants of the different functionalized graphenes, as decomposed into their purely electronic and vibrational contributions. By comparing the Si-doped with the Ge-doped case, the electronic contribution to C_{11} and C_{22} is seen to be very similar (311 versus 300 N/m); on the contrary, the vibrational contribution is found to be rather different in the two cases, with much larger values for Ge-doped than Si-doped graphene. This is a clear confirmation of the larger $\partial^2 H/(\partial \eta_v \partial Q_p)$ coupling in the former case.

As per Sn-doped graphene, from Figure 4 we see that its out-of-plane piezoelectricity is relatively small (2.8×10^{-10} C/m and 1.5 pm/V for e_{31} and d_{31}, respectively). This is basically due

Table 3: Elastic constants (in N/m) of Si-, Ge-, Sn- and pyrrolic N-doped graphene, at x=0.125. Electronic and vibrational contributions are separately reported. Dashes refer to null value of C_s-symmetry structures.

	Electronic				Vibrational			
	Si	Ge	Sn	H-NG	Si	Ge	Sn	H-NG
C_{11}	311	301	238	247	−60	−139	−81	−186
C_{22}	311	300	238	274	−59	−137	−57	−178
C_{12}	60	58	64	52	−16	−82	−32	−27
C_{16}	-	-	-	−20	-	-	-	13
C_{66}	125	121	63	95	−21	−27	−39	−69

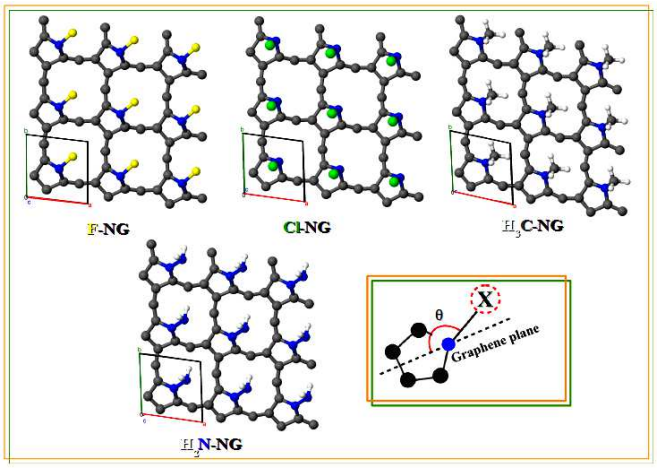

Figure 5: Graphical representation of the equilibrium configuration of pyrrolic N-doped graphene where H atoms are substituted with other functional groups (F-,Cl-, H_3C- and H_2N-). The inset provides a graphical definition of the θ angle.

to the large deformation angle δ of 42.1°, which makes the vibrationally-assisted penetration of Sn atoms into the graphene plane more difficult and the corresponding induced polarization small ($\mathscr{I}_p(z)$ = 0.52 km/mol). Furthermore, the vibration wavenumber of the soft phonon mode is large ($\bar{\nu}$ = 255 cm^{-1}) if compared to the other functionalizations. The case of the pyrrolic N-doping of graphene will be discussed below into detail in Section .

Pyrrolic N-doped Graphene

From inspection of Figure 4, the pyrrolic form of N-doped graphene (H-NG) is seen to exhibit a smaller out-of-plane piezoelectric response than Si- and Ge-doped graphenes and a larger one than Sn-doped graphene. In order to increase the piezoelectric response of pyrrolic N-doped graphene, different substitutions of the H atoms with F and Cl atoms or with methyl H_3C and amino H_2N groups are considered as model compounds, having the purpose in mind of softening the out-of-plane vibration mode and of increasing the corresponding induced polarization. A graphical representation of the equilibrium configurations of such functionalizations is given in Figure 5, where an angle θ is graphically defined to measure the position of the substituted group with respect to the graphene plane. As θ approaches the value of 180°, the substituted group lies horizontally to the plane and can largely penetrate into it by vibration, thus inducing a large polarization. On the contrary, when θ tends to 90°, the substituted group points perpendicularly out of the plane with corresponding low penetration and induced polarization. The θ angle is found to affect the piezoelectric response of pyrrolic N-doped graphene much more than the δ angle measuring the protrusion of the nitrogen atoms off the plane. Then, from Figure 6, panal (a), that reports the value of θ for different substitutions in pyrrolic N-doped graphene, one would expect Cl-NG to show the lowest piezoelectricity given that θ=92°. Indeed, due to their large atomic size, Cl atoms are the only ones to be stable in top site positions, while all other groups are found in hollow site positions. This is confirmed by present calculations, as reported in Table 4, where Cl-NG is seen to provide the smallest absolute values of piezoelectricity among all the functionalizations. This finding agrees with the previously reported piezoelectric values for light atom adsorptions on graphene, where hollow site adsorptions (Li, K, and LiF) showed higher piezoelectric constants than top site ones (H, F, and HF).[16]

A graphical representation of the atomic displacements involved in the soft phonon mode for each equilibrium configuration, as well as values of $\bar{\nu}$ for the different substitutions in pyrrolic N-doped graphene are reported in Figure 6, panals (b) and (c), respectively. The softest phonon modes are found in F-, H_3C- and H_2N-substituted systems. However, for the F-substitution, the induced

Table 4: Out-of-plane direct and converse piezoelectric constants (total values in units of 10^{-10} C/m and pm/V, respectively) for the substituted pyrrolic N-doped graphene.

	H	F	Cl	H_3C	H_2N
Direct					
e_{31}	11.81	6.87	2.83	-18.56	-27.29
e_{32}	12.83	10.38	3.04	-15.48	-12.25
e_{36}	-5.73	-2.9	-0.31	-2.47	-6.64
Converse					
d_{31}	13.53	-0.94	0.88	-23.79	-38.19
d_{32}	9.09	11.20	2.14	-5.88	0.59
d_{36}	-16.63	-20.80	-2.36	-30.83	-53.33

polarization is also decreased because of the higher electronegativity of F atoms. The methyl and amino group substitutions are then expected to provide the largest out-of-plane piezoelectric response, which is confirmed in Table 4.

To conclude, let us compare the absolute value of the piezoelectricity of the best systems we have been discussing in the present study (GeG and H_2N-NG), at the finite $x = 0.125$ concentration, with that of other 2D and 3D piezoelectric systems. For instance, the out-of-plane piezoelectricity of Ge-doped graphene and H_2N-NG are 50 and 10 times larger than the in-plane experimentally measured one of the h-MoS_2 monolayer.[8] These values are respectively 300 and 50 times larger

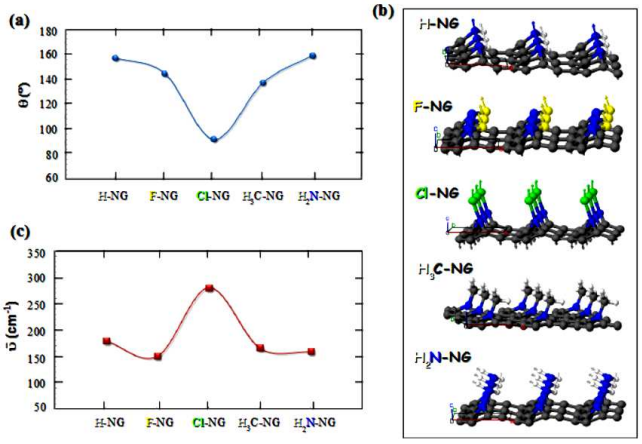

Figure 6: (a) Angle θ, (b) atomic displacements corresponding to the soft phonon mode and (c) phonon wave-number $\bar{\nu}$, for the different substitutions in pyrrolic N-doped graphene.

than the out-of-plane one induced by Li adsorption on graphene. Furthermore, present converse piezoelectric constants d_{31} are up to one and two orders of magnitude larger than those of bulk materials like quartz ($d_{11} = 2.3$ pm/V),[57] $Si_{0.83}Ge_{0.16}O_2$ ($d_{11} = 5.5$ pm/V),[47] GaN ($d_{33} = 3.7$ pm/V),[58] AlN ($d_{33} = 5.6$ pm/V),[58] and favorably compare to those of conventional lead zirconate titanate piezoelectric materials.[59]

Concluding Remarks

A quantum-mechanical rationalization of the microscopic mechanisms behind the induction of a piezoelectric response in graphene has been presented. Different kinds of chemical doping of graphene are considered, such as carbon atom substitutions with Si, Ge and Sn atoms and the pyrrolic form of N-doping as functionalized with different simple groups, which lead to non centro-symmetric non-planar equilibrium structures. On the one hand, the in-plane piezoelectric effect is seen to be i) dominated by the electronic response; ii) independent of the particular chemical or physical nature of the symmetry-breaking defects in the limit of small defect concentration, where it shows a finite value of about 5×10^{-10} C/m. On the other hand, the out-of-plane piezoelectricity is documented to i) be dominated by the vibrational rather than electronic contribution; ii) strongly depend upon the particular nature of the functionalization, with a response that vanishes as the defect concentration decreases in all cases. In order to produce a large out-of-plane piezoelectric effect in graphene, an optimal functionalization should involve the breaking of the inversion symmetry of pristine graphene and a soft IR active phonon mode with a large coupling with the cell deformation.

It is worth stressing that in the present investigation, one-sided protruded configurations only have been considered. Indeed, while two-sided configurations could still produce a non-null in-plane piezoelectric response, this would not be the case for the out-of-plane one, which would be progressively reduced and would eventually vanish for a balanced distribution of protrusions on the two sides of the graphene sheet. A second assumption that has been made in this study

was that of considering a regular distribution of defects. While an explicit study of the effect on the piezoelectric response of irregularly distributed patterns of interacting defects (which could be thermodynamically driven to group together) would certainly deserve further investigation, we might notice that some of the configurations that have been explored in the present study, with a low defect concentration, are characterized by non-interacting defects and yet by a large piezoelectric response.

Acknowledgement

El-Kelany acknowledges the Egyptian government for supporting his work at the Université de Pau et des Pays de l'Adour in France with a grant. The authors gratefully acknowledge the Centre Informatique National de l'Enseignement Supérieur (CINES) for computing facilities. The authors declare no competing financial interest.

References

(1) Wang, X.; Song, J.; Zhang, F.; He, C.; Hu, Z.; Wang, Z. Electricity Generation Based on One-Dimensional Group-III Nitride Nanomaterials. *Adv. Mater.* **2010**, *22*, 2155–2158.

(2) Nechibvute, A.; Chawanda, A.; Luhanga, P. Piezoelectric Energy Harvesting Devices: An Alternative Energy Source for Wireless Sensors. *Smart Materials Research* **2012**, *2012*, 853481.

(3) Madden, J. D.; Vandesteeg, N. A.; Anquetil, P. A.; Madden, P. G.; Takshi, A.; Pytel, R. Z.; Lafontaine, S. R.; Wieringa, P. A.; Hunter, I. W. Artificial Muscle Technology: Physical Principles and Naval Prospects. *IEEE J. Oceanic Eng.* **2004**, *29*, 706–728.

(4) Gautschi, G. *Piezoelectric Sensorics: Force, Strain, Pressure, Acceleration and Acoustic Emission Sensors, Materials and Amplifiers*; Engineering online library; Springer, 2002.

(5) Xiang, H. J.; Yang, J.; Hou, J. G.; Zhu, Q. Piezoelectricity in ZnO Nanowires: A First-principles Study. *Appl. Phys. Lett.* **2006**, *89*, 223111.

(6) Duerloo, K.-A. N.; Ong, M. T.; Reed, E. J. Intrinsic Piezoelectricity in Two-Dimensional Materials. *J. Phys. Chem. Lett.* **2012**, *3*, 2871–2876.

(7) Wu, W.; Wang, L.; Li, Y.; Zhang, F.; Lin, L.; Niu, S.; Chenet, D.; Zhang, X.; Hao, Y.; Heinz, T. F.; Hone, J.; Wang, Z. L. Piezoelectricity of Single-atomic-layer MoS_2 for Energy Conversion and Piezotronics. *Nature* **2014**, *514*, 470–474.

(8) Zhu, H.; Wang, Y.; Xiao, J.; Liu, M.; Xiong, S.; Wong, Z. J.; Ye, Z.; Ye, Y.; Yin, X.; Zhang, X. Observation of Piezoelectricity in Free-standing Monolayer MoS_2. *Nat. Nano* **2015**, *10*, 151–155.

(9) Novoselov, K. S.; Geim, A. K.; Morozov, S. V.; Jiang, D.; Katsnelson, M. I.; Grigorieva, I. V.; Dubonos, S. V.; Firsov, A. A. Two-Dimensional Gas of Massless Dirac Fermions in Graphene. *Nature* **2005**, *438*, 197–200.

(10) Novoselov, K. S.; Geim, A. K.; Morozov, S. V.; Jiang, D.; Zhang, Y.; Dubonos, S. V.; Grigorieva, I. V.; Firsov, A. A. Electric Field Effect in Atomically Thin Carbon Films. *Science* **2004**, *306*, 666–669.

(11) Bolotin, K. I.; Ghahari, F.; Shulman, M. D.; Stormer, H. L.; Kim, P. Observation of the Fractional Quantum Hall Effect in Graphene. *Nature* **2009**, *462*, 196–199.

(12) Cheng, R.; Bai, J.; Liao, L.; Zhou, H.; Chen, Y.; Liu, L.; Lin, Y.-C.; Jiang, S.; Huang, Y.; Duan, X. High-frequency Self-Aligned Graphene Transistors with Transferred Gate Stacks. *Proc. Nat. Acad. Sci.* **2012**, *109*, 11588–11592.

(13) Wu, Y.; Jenkins, K. A.; Valdes-Garcia, A.; Farmer, D. B.; Zhu, Y.; Bol, A. A.; Dimitrakopoulos, C.; Zhu, W.; Xia, F.; Avouris, P.; Lin, Y.-M. State-of-the-Art Graphene High-Frequency Electronics. *Nano Lett.* **2012**, *12*, 3062–3067.

(14) Bonaccorso, F.; Sun, Z.; Hasan, T.; Ferrari, A. C. Graphene Photonics and Optoelectronics. *Nat. Photon.* **2010**, *4*, 611–622.

(15) Dlubak, B.; Martin, M.-B.; Deranlot, C.; Servet, B.; Xavier, S.; Mattana, R.; Sprinkle, M.; Berger, C.; De Heer, W. A.; Petroff, F.; Anane, A.; Seneor, P.; Fert, A. Highly Efficient Spin Transport in Epitaxial Graphene on SiC. *Nat. Phys.* **2012**, *8*, 557–661.

(16) Ong, M. T.; Reed, E. J. Engineered Piezoelectricity in Graphene. *ACS Nano* **2012**, *6*, 1387–1394.

(17) Chandratre, S.; Sharma, P. Coaxing Graphene to be Piezoelectric. *Appl. Phys. Lett.* **2012**, *100*, 023114.

(18) Zelisko, M.; Hanlumyuang, Y.; Yang, S.; Liu, Y.; Lei, C.; Li, J.; Ajayan, P. M.; Sharma, P. Anomalous Piezoelectricity in Two-dimensional Graphene Nitride Nanosheets. *Nat. Commun.* **2014**, *5*, 1–7.

(19) Wang, X.; Tian, H.; Xie, W.; Shu, Y.; Mi, W.-T.; Ali Mohammad, M.; Xie, Q.-Y.; Yang, Y.; Xu, J.-B.; Ren, T.-L. Observation of a Giant Two-dimensional Band-piezoelectric Effect on Biaxial-strained Graphene. *NPG Asia Mater.* **2015**, *7*, e154.

(20) Rodrigues, G. d. C.; Zelenovskiy, P.; Romanyuk, K.; Luchkin, S.; Kopelevich, Y.; Kholkin, A. Strong Piezoelectricity in Single-layer Graphene Deposited on SiO_2 Grating Substrates. *Nat. Commun.* **2015**, *6*, 1–6.

(21) El-Kelany, K. E.; Carbonnière, P.; Erba, A.; Rérat, M. Inducing a Finite In-Plane Piezoelectricity in Graphene with Low Concentration of Inversion Symmetry-Breaking Defects. *J. Phys. Chem. C* **2015**, *119*, 8966–8973.

(22) Shi, Y.; Kim, K. K.; Reina, A.; Hofmann, M.; Li, L.-J.; Kong, J. Work Function Engineering of Graphene Electrode via Chemical Doping. *ACS Nano* **2010**, *4*, 2689–2694, PMID: 20433163.

(23) Ci, L.; Song, L.; Jin, C.; Jariwala, D.; Wu, D.; Li, Y.; Srivastava, A.; Wang, Z. F.; Storr, K.;

Balicas, L.; Liu, F.; Ajayan, P. M. Atomic Layers of Hybridized Boron Nitride and Graphene Domains. *Nat. Mater.* **2010**, *9*, 430–435.

(24) Liu, M.; Li, Y.; Chen, P.; Sun, J.; Ma, D.; Li, Q.; Gao, T.; Gao, Y.; Cheng, Z.; Qiu, X.; Fang, Y.; Zhang, Y.; Liu, Z. Quasi-Freestanding Monolayer Heterostructure of Graphene and Hexagonal Boron Nitride on Ir(111) with a Zigzag Boundary. *Nano Lett.* **2014**, *14*, 6342–6347.

(25) Panchakarla, L. S.; Subrahmanyam, K. S.; Saha, S. K.; Govindaraj, A.; Krishnamurthy, H. R.; Waghmare, U. V.; Rao, C. N. R. Synthesis, Structure, and Properties of Boron- and Nitrogen-Doped Graphene. *Adv. Mater.* **2009**, *21*, 4726–4730.

(26) Lv, R.; Li, Q.; Botello-Méndez, A. R.; Hayashi, T.; Wang, B.; Berkdemir, A.; Hao, Q.; Elías, A. L.; Cruz-Silva, R.; Gutiérrez, H. R. et al. Nitrogen-doped Graphene: Beyond Single Substitution and Enhanced Molecular Sensing. *Sci. Rep.* **2012**, *2*, 1–8.

(27) Lv, R.; dos Santos, M. C.; Antonelli, C.; Feng, S.; Fujisawa, K.; Berkdemir, A.; Cruz-Silva, R.; Elías, A. L.; Perea-Lopez, N.; López-Urías, F.; Terrones, H.; Terrones, M. Large-Area Si-Doped Graphene: Controllable Synthesis and Enhanced Molecular Sensing. *Adv. Mater.* **2014**, *26*, 7593–7599.

(28) Chang, C.-K.; Kataria, S.; Kuo, C.-C.; Ganguly, A.; Wang, B.-Y.; Hwang, J.-Y.; Huang, K.-J.; Yang, W.-H.; Wang, S.-B.; Chuang, C.-H. et al. Band Gap Engineering of Chemical Vapor Deposited Graphene by in Situ BN Doping. *ACS Nano* **2013**, *7*, 1333–1341.

(29) Wang, H.; Maiyalagan, T.; Wang, X. Review on Recent Progress in Nitrogen-Doped Graphene: Synthesis, Characterization, and Its Potential Applications. *ACS Catal.* **2012**, *2*, 781–794.

(30) Long, D.; Li, W.; Ling, L.; Miyawaki, J.; Mochida, I.; Yoon, S.-H. Preparation of Nitrogen-Doped Graphene Sheets by a Combined Chemical and Hydrothermal Reduction of Graphene Oxide. *Langmuir* **2010**, *26*, 16096–16102.

(31) Deng, D.; Pan, X.; Yu, L.; Cui, Y.; Jiang, Y.; Qi, J.; Li, W.-X.; Fu, Q.; Ma, X.; Xue, Q.; Sun, G.; Bao, X. Toward N-Doped Graphene via Solvothermal Synthesis. *Chemistry of Materials* **2011**, *23*, 1188–1193.

(32) King-Smith, R. D.; Vanderbilt, D. Theory of Polarization of Crystalline Solids. *Phys. Rev. B* **1993**, *47*, 1651–1654.

(33) Vanderbilt, D. Berry-Phase Theory of Proper Piezoelectric Response. *J. Phys. Chem. Solids* **2000**, *61*, 147–151.

(34) Resta, R. Macroscopic Polarization in Crystalline Dielectrics: the Geometric Phase Approach. *Rev. Mod. Phys.* **1994**, *66*, 899–915.

(35) Noël, Y.; Zicovich-Wilson, C. M.; Civalleri, B.; D'Arco, P.; Dovesi, R. Polarization Properties of ZnO and BeO: An Ab initio Study Through the Berry Phase and Wannier Functions Approaches. *Phys. Rev. B* **2001**, *65*, 014111.

(36) Erba, A.; El-Kelany, K. E.; Ferrero, M.; Baraille, I.; Rérat, M. Piezoelectricity of $SrTiO_3$: An Ab initio Description. *Phys. Rev. B* **2013**, *88*, 035102.

(37) Dovesi, R.; Orlando, R.; Erba, A.; Zicovich-Wilson, C. M.; Civalleri, B.; Casassa, S.; Maschio, L.; Ferrabone, M.; De La Pierre, M.; D'Arco, Ph.; Noël, Y.; Causá, M.; Rérat, M.; Kirtman, B. CRYSTAL14: A Program for the Ab initio Investigation of Crystalline Solids. *Int. J. Quantum Chem.* **2014**, *114*, 1287–1317.

(38) Dovesi, R.; Saunders, V. R.; Roetti, C.; Orlando, R.; Zicovich-Wilson, C. M.; Pascale, F.; Doll, K.; Harrison, N. M.; Civalleri, B.; Bush, I. J.; D'Arco, P.; Llunell, M.; Causà, M.; Noël, Y. `CRYSTAL14` User's Manual. 2013; http://www.crystal.unito.it.

(39) Becke, A. D. Density-Functional Exchange-Energy Approximation with Correct Asymptotic Behavior. *Phys. Rev. A* **1988**, *38*, 3098–3100.

(40) Peintinger, M. F.; Oliveira, D. V.; Bredow, T. Consistent Gaussian Basis Sets of Triple-Zeta Valence with Polarization Quality for Solid-State Calculations. *J. Comp. Chem.* **2013**, *34*, 451–459.

(41) Causà, M.; Dovesi, R.; Roetti, C. Pseudopotential Hartree-Fock Study of Seventeen III-V and IV-IV Semiconductors. *Phys. Rev. B* **1991**, *43*, 11937–11943.

(42) Erba, A.; Mahmoud, A.; Orlando, R.; Dovesi, R. Elastic Properties of Six Silicate Garnet End-members from Accurate Ab initio Simulations. *Phys. Chem. Min.* **2014**, *41*, 151–160.

(43) Tan, J. C.; Civalleri, B.; Erba, A.; Albanese, E. Quantum Mechanical Predictions to Elucidate the Anisotropic Elastic Properties of Zeolitic Imidazolate Frameworks: ZIF-4 vs. ZIF-zni. *CrystEngComm* **2015**, *17*, 375–382.

(44) Erba, A.; Dovesi, R. Photoelasticity of Crystals from Theoretical Simulations. *Phys. Rev. B* **2013**, *88*, 045121.

(45) Erba, A.; Ruggiero, M. T.; Korter, T. M.; Dovesi, R. Piezo-Optic Tensor of Crystals from Quantum-Mechanical Calculations. *J. Chem. Phys.* **2015**, *143*, 144504.

(46) Mahmoud, A.; Erba, A.; El-Kelany, K. E.; Rérat, M.; Orlando, R. Low-Temperature Phase of $BaTiO_3$: Piezoelectric, Dielectric, Elastic, and Photo Elastic Properties from Ab initio Simulations. *Phys. Rev. B* **2014**, *89*, 045103.

(47) El-Kelany, K. E.; Erba, A.; Carbonnière, P.; Rérat, M. Piezoelectric, Elastic, Structural and Dielectric Properties of $Si_{1-x}Ge_xO_2$ Solid Solution: a Theoretical Study. *J. Phys.: Cond. Matter* **2014**, *26*, 205401.

(48) Erba, A.; Ferrabone, M.; Baima, J.; Orlando, R.; Rérat, M.; Dovesi, R. The Vibration Properties of the (n,0) Boron Nitride Nanotubes from Ab initio Quantum Chemical Simulations. *J. Chem. Phys.* **2013**, *138*, 054906.

(49) Lacivita, V.; Erba, A.; Noël, Y.; Orlando, R.; D'Arco, Ph.; Dovesi, R. Zinc Oxide Nanotubes: An Ab initio Investigation of Their Structural, Vibrational, Elastic, and Dielectric Properties. *J. Chem. Phys.* **2013**, *138*, 214706.

(50) Baima, J.; Erba, A.; Orlando, R.; Rérat, M.; Dovesi, R. Beryllium Oxide Nanotubes and Their Connection to the Flat Monolayer. *J. Phys. Chem. C* **2013**, *117*, 12864–12872.

(51) Baima, J.; Erba, A.; Maschio, L.; Zicovich-Wilson, C.; Dovesi, R.; Kirtman, B. Direct Piezoelectric Tensor of 3D Periodic Systems through a Coupled Perturbed Hartree-Fock/Kohn-Sham Method. *Z. Phys. Chem.* **2015**, DOI: 10.1515/zpch-2015-0701.

(52) Xiu, S. L.; Gong, L.; Wang, V.; Liang, Y. Y.; Chen, G.; Kawazoe, Y. Degenerate Perturbation in Band-Gap Opening of Graphene Superlattice. *J. Phys. Chem. C* **2014**, *118*, 8174–8180.

(53) Lambin, P.; Amara, H.; Ducastelle, F.; Henrard, L. Long-Range Interactions Between Substitutional Nitrogen Dopants in Graphene: Electronic Properties Calculations. *Phys. Rev. B* **2012**, *86*, 045448.

(54) Martinazzo, R.; Casolo, S.; Tantardini, G. F. Symmetry-Induced Band-Gap Opening in Graphene Superlattices. *Phys. Rev. B* **2010**, *81*, 245420.

(55) Grupp, D. E.; Goldman, A. M. Giant Piezoelectric Effect in Strontium Titanate at Cryogenic Temperatures. *Science* **1997**, *276*, 392–394.

(56) Wu, X.; Vanderbilt, D.; Hamann, D. Systematic Treatment of Displacements, Strains, and Electric Fields in Density-functional Perturbation Theory. *Phys. Rev. B* **2005**, *72*, 035105.

(57) Bechmann, R. Elastic and Piezoelectric Constants of Alpha-Quartz. *Phys. Rev.* **1958**, *110*, 1060–1061.

(58) Guy, I. L.; Muensit, S.; Goldys, E. M. Extensional Piezoelectric Coefficients of Gallium Nitride and Aluminum Nitride. *Appl. Phys. Lett.* **1999**, *75*, 4133–4135.

(59) Guo, Q.; Cao, G. Z.; Shen, I. Y. Measurements of Piezoelectric Coefficient d_{33} of Lead Zirconate Titanate Thin Films Using a Mini Force Hammer. *J. Vib. Acoust.* **2013**, *135*, 011003.